Non-linear bulk micromachined accelerometer for high sensitivity applications

Middelburg, L.M.; Mansouri, B. El; Poelma, Rene; Zhang, G.Q.; van Zeijl, Henk; Wei, Jia

DOI
10.1109/ICSENS.2018.8589630

Publication date
2018

Document Version
Accepted author manuscript

Published in
2018 IEEE SENSORS Proceedings

Non-linear bulk micromachined accelerometer for high sensitivity applications

L.M. Middelburg[1], B. El Mansouri[1], Rene Poelma[1], G.Q. Zhang[1], Henk van Zeijl[1], Jia Wei[2]
[1]Electronic Components, Technology and Materials, Faculty of Electrical Engineering, Delft University of Technology, Mekelweg 4, 2628CD, Delft, The Netherlands
[2]Else Kooi Laboratory, Feldmannweg 17, 2628CT, Delft, The Netherlands

***Abstract*—This work describes the design, modelling and realisation of the mechanical part of a non-linear MEMS accelerometer intended for large displacement behaviour. For this, a mass/spring system was designed with an extremely low resonance frequency. In this work the mechanical behaviour was verified by measurements done using an optical setup, including a laser and photodiode. The results are a resonance frequency of 12.6 Hz, which can be further tuned depending on the application by varying the mass, beam thickness and tilt of the structure. This results in a mechanical sensitivity of 0.16 [mm/ms^{-2}]. The future goal of this work is to integrate a read-out scheme on wafer level, for example electrostatically.**

Keywords—non-linear MEMS; accelerometer; optical read-out; large displacement behaviour.

I. INTRODUCTION

Recently, non-linear behaviour in MEMS devices have attracted more attention. The exploitation of non-linear effects in the mechanical behaviour of devices such as an accelerometer can yield the advantage of an extremely high sensitivity, at the expense of a smaller dynamic range. In various applications, the dynamic range can be reduced for this purpose, especially with the trend of Internet of Things (IoT) [1], where sensors will be omnipresent and interconnected.

The starting point for the mechanical design of this work is based on a paper written by Middlemiss et. Al. [2, 3]. In this paper the non-linear behaviour of large displacement compliant systems [4] is used to design for a locally low stiffness of the spring. However, the device presented by Middlemiss [2, 3] only has three beams to support the moving mass which may result in rotational motion. To measure movement of the mass accurately, an uniform vertical motion is required. The aim of this work is therefore to redesign and characterize the mechanical part with four beams. The redesigned device is aimed for integration of an on chip readout in future iterations of the device.

The mass/spring system can be designed in such a way that the mass is 'biased' at the point of this low spring constant, yielding a relative open-loop accelerometer with high mechanical sensitivity. The unique feature this design to measure accurate g-variation with a biased 1g force. This is obtained by designing a non-linear beam with a linear stiffness region at a biased point.
The challenge in the design of the device is to align the mass-bias to the linear region of the beam.

Such devices can for example be used in monitoring deviations in the gravitational force of the earth [3] or vibration and motion analysis [5].

Advantages over existing designs lie in the requirements of the read-out of the displacement which can be largely relaxed, since a small acceleration signal on the proof mass is already resulting in a large displacement. This read-out can be done optically, as described in literature [3, 6] but in future designs also electrostatically such as was designed by Li [7]. Here a linear MEMS device was fabricated achieving a resonance frequency of 13.2 Hz accompanying a high sensitivity through the usage of coarse and fine capacitive sensing.

II. DESIGN

A. Mass/beam design

The design was constrained by a few factors. Firstly the objective was to perform bulk-micromachining on a silicon wafer, which fixed the height of the device to wafer thickness. Secondly, one of the objectives was to keep the die-size to an area of 10x10 mm^2. Because a low-resonance frequency was aimed for, a relatively large mass in combination with locally very compliant springs is required. The smallest beam width which was practically feasible was 5 [µm]. To make the beams fit within the restricted area, the beams were attached towards the centre of the proof mass. With this procedure, a trade-off is present between the torsional stiffness and the length of the beam, thus the stiffness. The mass/beam system is suspended in a frame, which was designed such that lateral space would be available for optical read-out or future integration of other transducer types.

Because of the non-linear nature of the springs, the design was aided with finite element analysis (FEA) simulations. Design parameters were the beam length, beam width, sector angle, the rotation and the angles between the proof mass / frame and the beam itself. Fig. 1 shows the 2D simulation of a single beam in its deflected state. Because both ends are fixed, one on the frame, the other on the proof mass, the beam will show an S-shape when it is deflected beyond a certain point while the proof mass is moving in a straight line without any torsional movements. Choosing the right values for the design parameters gives the desired force-displacement behaviour, in which it is important to avoid any negative stiffness. Negative stiffness would result in the existence of two values for the deflection (x) for the same force (F) which can result in snap-through behaviour. Moreover, this effect is generally undesired

because it introduces dis-ambiguity when displacement values are read-out. The simulated force/displacement behaviour of the beam showing clear spring softening is included in Fig. 2. It can be clearly noticed that the spring softening effect occurs. When the mass is chosen such, that the spring is biased in the 'flat region' for the offset acceleration force, a low stiffness will be the result, implying a low resonance frequency.

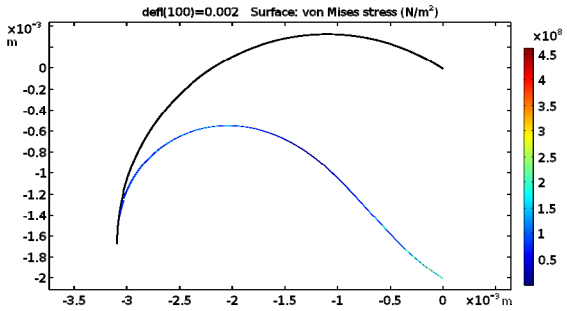

Fig. 1. A 2D simulation of a deformed beam. Only one beam is simulated to reduce computational power of the non-linear simulation.

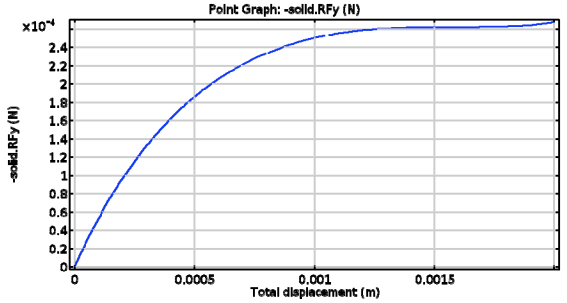

Fig. 2. The force displacement characteristic of the modelled beam. Note that spring softening occurs with increasing displacement, while no negative stiffness is exhibited.

III. Fabrication

The designed long thin beams will be fabricated by using Deep Reactive Ion Etching (DRIE), also known as Bosch process. The slope of the sidewalls can become an issue when very thin structures are considered. Therefore, before the mask was ordered, first test structures were fabricated and inspected to check the etch sidewall profile and thus the homogeneity of the beam width along the wafer thickness. Moreover, the inspection and handling of the cross section gives an insight in the feasibility of the extremely high aspect ratio (AR) and long beams. Images of a cross section were made of beams with a thickness of 3.4 and 13.8 [µm] respectively, using an optical microscope. Fig. 3 illustrates this. It was concluded from the inspection and measurements that the angle of the sidewall slope is approximating zero. Measured thickness variation was not measureable for the 3.4 [µm] beam. It was concluded from these in-line process inspections, that 5 µm wide beams would be feasible as described by the design. The fabrication was carried out using a 4 [µm] silicon oxide hard mask on a 300 [µm] thick double side polished wafer. As landing layer on the backside 3 [µm] silicon oxide was used followed by a 3 [µm] thick layer of AlSi(1 %) to prevent helium leakage in the case of cracks in the landing layer during DRIE etching. The hard mask was patterned using standard lithography followed by plasma etching.

Through wafer etch required two iterations to determine the exact number of loops needed. After DRIE etching, the organic passivation material and lithography masking layer of photo resist were removed to subsequently release the etched structures using a vapour hydrofluoric acid (HF) tool.

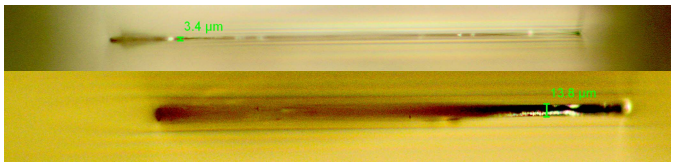

Fig. 3. To check feasibility and sidewall profile of bulk micromachined long thin beams, cross sections have been made of test structures. The high AR is clearly noticeable from the optical pictures.

Manual excitation was needed to fully release the halo-structured sacrificial pieces included in the mask design and etched in the silicon along with the mass/beam structures. A picture of the released mass/beam structures is included in Fig. 4. There has been chosen not to dice the devices in this work. Leaving the devices within the wafer is considered advantageous for handling during further testing. The mass/beam structures were shielded from the environment by using glass wafers on both sides with spacing in between to ensure the free movement of the mass/beam structures. An overview of the entire process flow is included in Fig. 5.

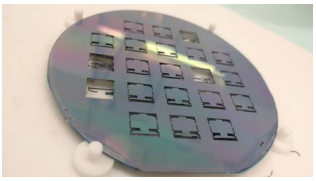

Fig. 4. Releasing the bulk micromachined structures using a Teflon carrier for the vapour HF tool.

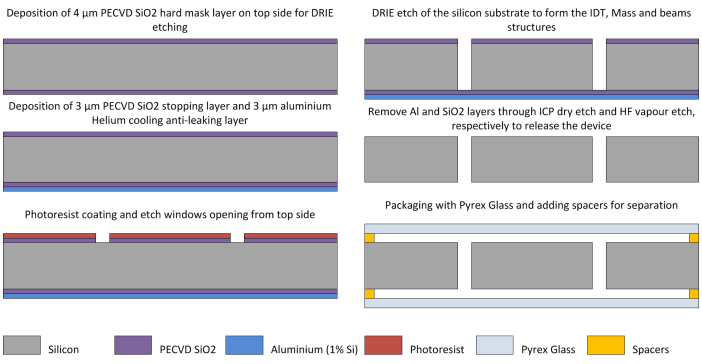

Fig. 5. An overview of the used process flow for making the devices.

IV. Measurement and Characterization

A. Measurement setup

An optical measurement setup was used consisting of a mechanical shaker driven by a shaker amplifier, in turn driven by a signal generator. The signal generator was used to perform a sweep of a sinusoidal frequency. The output of the signal generator is also fed to the Data Acquisition device from National Instruments (NI DAQ) and sampled using MATLAB. On the shaker, the entire wafer with the etched resonators is mounted. As soon as the proof mass of the sensor die starts to resonate caused by the mechanical excitation, the laser beam, which is in line with the edge of the proof mass, is subsequently transmitted through the glass covered die to the photodiode aligned behind the wafer. Both the wafer and the mass are moving with the amplitude of the shaker, however when resonance takes place the deflection of the mass within the etched openings is dramatically increased. As a result, the time intervals where the laser penetrates the sample get longer, resulting in increased response from the photo diode.

As a result is the transmission of the resonator a function of the movement of the proof mass. The measurement signal from the photodiode can therefore be used to form a mechanical spectrum and to detect the position of the resonance frequency of the first Eigenmode. Technical details on the measurement setup are included in TABLE I.

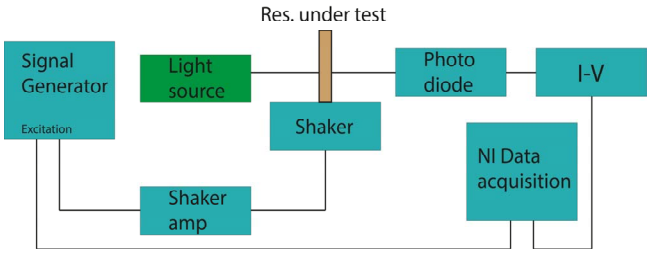

Fig. 6. A schematic overview of the measurement setup used to optically characterize the resonators.

TABLE I. Measurement Equipment

Device	Make, model
Signal generator	Agilent
Power amplifier shaker	Brüel & Kjaer 2718
Mechanical shaker	Brüel & Kjaer 4810
Laser	Melles Griot 633nm
Photodiode	Texas Instruments OPT101P
DAQ-device	NI DAQ USB-6210

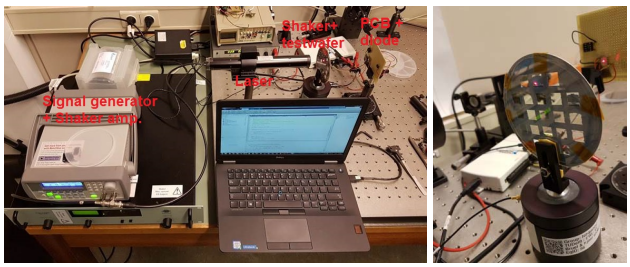

Fig. 7. Pictures of the measurement setup. The bulk micro machined wafer is clearly visible.

B. Results

To verify if the resonance frequency lies on the desired position in the mechanical spectrum, a sweep was carried out from 5 to 15 [Hz]. Because some energy is needed to get the resonating mass into resonance, the sweep time was chosen to be 60 [s] and the sample rate used was 1 [ks/s]. Two measurements on the same die were carried out. The time domain signal was read with the aid of MATLAB, after which a Fast Fourier Transform (FFT) was performed to determine the spectrum. The result is included in Fig. 8. The absolute value of the spectral plot is influenced largely by the intensity of the laser, the type of photo diode and the output power of the shaker amplifier. This is not considered as an issue since the location of the resonance peak of the first Eigen Mode is of main interest during these measurements. The measured resonance frequency equals 12.6 Hz for both measurements, corresponding to a mechanical sensitivity of 0.4 [mm/ms^{-2}]. Based on the -3 [dB] frequency, the Q-factor of the device was determined to be 12.0.

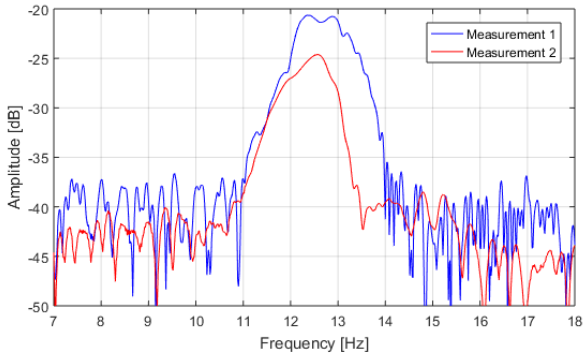

Fig. 8. Two measurement results for the same measured sensor die. Resonance frequency is constant at 12.6 [Hz] for both measurements.

V. Conclusion

A mass/spring system was designed, fabricated and characterized with the aid of an optical measurement setup. The non-linear properties of slender beams incorporated in compliant systems were exploited to yield an inertial sensor with a large mechanical sensitivity. This can be used to function as a starting point for an open-loop relative MEMS accelerometer with a high input-referred system resolution intended for vibration monitoring or measurements of earth gravitational fields. Future work therefore includes the development of an integrated read-out transducer, which can be optically, electrostatic, or any other implementation fitting the existing design.

Acknowledgment

This work was supported by the European project "IoSense: Flexible FE/BE Sensor Pilot Line for the Internet of Everything". This project has received funding from the Electronic Component Systems for European Leadership Joint Undertaking under grant agreement No 692480. Furthermore, the authors would like to thank Dr.ir. J.G. Vogel for the help and assistance with the modelling and measurement setup.

REFERENCES

[1] Atzori, L., Iera, A., and Morabito, G.: 'The internet of things: A survey', Computer networks, 2010, 54, (15), pp. 2787-2805

[2] Middlemiss, R., Samarelli, A., Paul, D., Hough, J., Rowan, S., and Hammond, G.: 'Measurement of the Earth tides with a MEMS gravimeter', Nature, 2016, 531, (7596), pp. 614

[3] Middlemiss, R.P., Bramsiepe, S.G., Douglas, R., Hough, J., Paul, D.J., Rowan, S., and Hammond, G.D.: 'Field Tests of a Portable MEMS Gravimeter', Sensors, 2017, 17, (11), pp. 2571

[4] Howell, L.L.: 'Compliant mechanisms' (John Wiley & Sons, 2001. 2001)

[5] Amini, B.V., and Ayazi, F.: 'Micro-gravity capacitive silicon-on-insulator accelerometers', Journal of Micromechanics and Microengineering, 2005, 15, (11), pp. 2113

[6] Krishnan, G., Kshirsagar, C.U., Ananthasuresh, G., and Bhat, N.: 'Micromachined high-resolution accelerometers', Journal of the Indian Institute of Science, 2012, 87, (3), pp. 333

[7] Li, Z., Wu, W.J., Zheng, P.P., Liu, J.Q., Fan, J., and Tu, L.C.: 'Novel capacitive sensing system design of a microelectromechanical systems accelerometer for gravity measurement applications', Micromachines, 2016, 7, (9), pp. 167

1 Atzori, L., Iera, A., and Morabito, G.: 'The internet of things: A survey', Computer networks, 2010, 54, (15), pp. 2787-2805

2 Middlemiss, R., Samarelli, A., Paul, D., Hough, J., Rowan, S., and Hammond, G.: 'Measurement of the Earth tides with a MEMS gravimeter', Nature, 2016, 531, (7596), pp. 614

3 Middlemiss, R.P., Bramsiepe, S.G., Douglas, R., Hough, J., Paul, D.J., Rowan, S., and Hammond, G.D.: 'Field Tests of a Portable MEMS Gravimeter', Sensors, 2017, 17, (11), pp. 2571

4 Howell, L.L.: 'Compliant mechanisms' (John Wiley & Sons, 2001. 2001)

5 Amini, B.V., and Ayazi, F.: 'Micro-gravity capacitive silicon-on-insulator accelerometers', Journal of Micromechanics and Microengineering, 2005, 15, (11), pp. 2113

6 Krishnan, G., Kshirsagar, C.U., Ananthasuresh, G., and Bhat, N.: 'Micromachined high-resolution accelerometers', Journal of the Indian Institute of Science, 2012, 87, (3), pp. 333

7 Li, Z., Wu, W.J., Zheng, P.P., Liu, J.Q., Fan, J., and Tu, L.C.: 'Novel Capacitive Sensing System Design of a Microelectromechanical Systems Accelerometer for Gravity Measurement Applications', Micromachines, 2016, 7, (9), pp. 167